



ELSEVIER

Contents lists available at ScienceDirect

## Brain Stimulation

journal homepage: <http://www.journals.elsevier.com/brain-stimulation>

## The sensitivity of ECG contamination to surgical implantation site in brain computer interfaces



Wolf-Julian Neumann<sup>a,\*</sup>, Majid Memarian Sorkhabi<sup>b</sup>, Moaad Benjaber<sup>b</sup>, Lucia K. Feldmann<sup>a</sup>, Assel Saryyeva<sup>c</sup>, Joachim K. Krauss<sup>c</sup>, Maria Fiorella Contarino<sup>d,e</sup>, Tomas Sieger<sup>f</sup>, Robert Jech<sup>f</sup>, Gerd Tinkhauser<sup>g</sup>, Claudio Pollo<sup>h</sup>, Chiara Palmisano<sup>i</sup>, Ioannis U. Isaias<sup>i</sup>, Daniel D. Cummins<sup>j</sup>, Simon J. Little<sup>j</sup>, Philip A. Starr<sup>k</sup>, Vasileios Kokkinos<sup>l</sup>, Schneider Gerd-Helge<sup>m</sup>, Todd Herrington<sup>n</sup>, Peter Brown<sup>b</sup>, R. Mark Richardson<sup>l</sup>, Andrea A. Kühn<sup>a</sup>, Timothy Denison<sup>b</sup>

<sup>a</sup> Movement Disorder and Neuromodulation Unit, Department of Neurology, Charité - Universitätsmedizin Berlin, Chariteplatz 1, 10117, Berlin, Germany

<sup>b</sup> MRC Brain Network Dynamics Unit, Nuffield Department of Clinical Neurosciences, University of Oxford, United Kingdom

<sup>c</sup> Department of Neurosurgery, Medizinische Hochschule Hannover, Hannover, Germany

<sup>d</sup> Department of Neurology, Leiden University Medical Center, Leiden, the Netherlands

<sup>e</sup> Department of Neurology, Haga Teaching Hospital, The Hague, the Netherlands

<sup>f</sup> Department of Neurology, Charles University, 1st Faculty of Medicine and General University Hospital, Prague, Czech Republic

<sup>g</sup> Department of Neurology, Bern University Hospital and University of Bern, Bern, Switzerland

<sup>h</sup> Department of Neurosurgery, Bern University Hospital and University of Bern, Bern, Switzerland

<sup>i</sup> Department of Neurology, University Hospital of Würzburg and Julius Maximilian University of Würzburg, Würzburg, Germany

<sup>j</sup> Department of Neurology, University of California, San Francisco, San Francisco, CA, 94143, USA

<sup>k</sup> Department of Neurological Surgery, University of California, San Francisco, San Francisco, CA, 94143, USA

<sup>l</sup> Department of Neurosurgery, Massachusetts General Hospital and Harvard Medical School, Boston, MA, USA

<sup>m</sup> Department of Neurosurgery, Charité - Universitätsmedizin Berlin, Chariteplatz 1, 10117, Berlin, Germany

<sup>n</sup> Department of Neurology, Massachusetts General Hospital and Harvard Medical School, Boston, MA, USA

### ARTICLE INFO

#### Article history:

Received 6 April 2021

Received in revised form

5 August 2021

Accepted 19 August 2021

Available online 21 August 2021

#### Keywords:

Deep brain stimulation

Brain computer interface

Oscillations

Artifacts

Neuromodulation

### ABSTRACT

**Background:** Brain sensing devices are approved today for Parkinson's, essential tremor, and epilepsy therapies. Clinical decisions for implants are often influenced by the premise that patients will benefit from using sensing technology. However, artifacts, such as ECG contamination, can render such treatments unreliable. Therefore, clinicians need to understand how surgical decisions may affect artifact probability.

**Objectives:** Investigate neural signal contamination with ECG activity in sensing enabled neuro-stimulation systems, and in particular clinical choices such as implant location that impact signal fidelity. **Methods:** Electric field modeling and empirical signals from 85 patients were used to investigate the relationship between implant location and ECG contamination.

**Results:** The impact on neural recordings depends on the difference between ECG signal and noise floor of the electrophysiological recording. Empirically, we demonstrate that severe ECG contamination was more than 3.2x higher in left-sided subclavicular implants (48.3%), when compared to right-sided implants (15.3%). Cranial implants did not show ECG contamination.

**Conclusions:** Given the relative frequency of corrupted neural signals, we conclude that implant location will impact the ability of brain sensing devices to be used for "closed-loop" algorithms. Clinical adjustments such as implant location can significantly affect signal integrity and need consideration.

© 2021 Published by Elsevier Inc. This is an open access article under the CC BY-NC-ND license (<http://creativecommons.org/licenses/by-nc-nd/4.0/>).

\* Corresponding author.

E-mail address: [julian.neumann@charite.de](mailto:julian.neumann@charite.de) (W.-J. Neumann).

## 1. Introduction

Invasive neurostimulation can modulate neural activity and alleviate symptoms in a variety of severe neurological and psychiatric disorders [1,2]. Current advances in deep brain stimulation (DBS) research demonstrate the utility of closed-loop adaptive DBS based on neural feedback signals recorded directly from the stimulation electrodes [3–6]. Most prominently, subthalamic beta activity (13–35 Hz) in Parkinson's disease was shown to reflect parkinsonian motor sign severity [7] that rapidly follows the clinical response to treatment [8–10] and is a promising candidate for adaptive deep brain stimulation (aDBS) [11,12]. Similarly, in patients with epilepsy, seizure activity can inform rapid therapeutic intervention [13]. In such scenarios, clinical success of demand-dependent therapy adaptation depends on the reliability of the feedback signal [14,15]. Neurophysiological recordings are prone to electrical artifacts. The strongest source of electrical activity in the human body is the heart, and the frequency content of cardiac activity overlaps many brain signals of interest (Fig. 1) [16]. Since the first experience with sensing enabled implantable DBS devices, ECG contamination remains an unresolved problem rendering a significant number of recordings unusable [17,18]. Similar issues may arise with motion and muscle contraction (see Supplementary Fig. 1). In the present study, we investigate the relationship between the electric field of cardiac activity, implant location, and contamination of neural signals recorded.

## 2. Methods

### 2.1. Empirical data

The study was carried out in accordance with the Declaration of Helsinki and was approved by the internal review board of Charité – Universitätsmedizin Berlin. To validate the predictions of our model, we visually inspected recordings for ECG contamination. Therefore, archival local field potential (LFP) recordings from 8 international neuromodulation centers in 86 implants in 85 patients were inspected for evidence of ECG. From this cohort, 53 patients have undergone implantation of Medtronic Percept DBS pulse generators (21 left subclavicular, 1 left abdomen, 29 right subclavicular, 1 right abdomen, 1 both left and right subclavicular; see Table 1). DBS was most commonly applied bilaterally (one lead in each hemisphere), 4 implants only had leads in one hemisphere connected (unilateral). Calibration tests were performed bipolarly for contact pairs 0–2 and 1–3, with 0 being the most distal contact. Importantly, these calibration tests are performed in passive recharge mode, with the stimulation anode set to the IPG and cathode defined as contacts 1 or 2 respectively, to simulate the recording montage required for stimulation without applying current [19]. The sensing configuration constrains the system to 2 channels per lead. One channel from one patient had to be excluded due to impedance issues, resulting in 207 channels overall. Additionally, 32 patients have been implanted with a neurostimulation system mounted to the skull (cranial mount) for treatment refractory epilepsy therapy (RNS Neuropace). For Percept data, bipolar calibration test recordings of ~20 s length were visualized using our open source Perceive Toolbox ([www.github.com/neuromodulation/perceive/](http://www.github.com/neuromodulation/perceive/)) in MATLAB (The MathWorks). For cranial mounts, visual inspection was performed from routine recordings. ECG artifacts were identified based on the presence of characteristic sharp QRS-like signal deflections of ~150–200 ms width with stereotypic amplitudes occurring at 60–100 bpm. Artifacts were categorized into absent, minor, and severe (see Fig. 1), as some recordings had visible but low amplitude contamination, e.g., with just the tip of the QRS complex close to the level of neural

activity. Statistical comparison of implant location and observed ECG contamination were performed by aggregating channel counts per implant and using the exact version of non-parametric Wilcoxon's rank sum tests. To confirm that ECG contamination in subclavicular implants is more likely with coupling of the stimulation anode to the IPG, we have compared recordings performed with the IPG coupled (ready for stimulation in calibration test mode) and uncoupled (not ready for stimulation in BrainSense Survey mode) in a sub-cohort of 13 patients (subject 1–9 and 1–4 of left/right chest implants) using Wilcoxon's signed rank test.

### 2.2. Modeling

Physiological modeling can be used to better understand the effect of the reference electrode placement on the induced cardiac artifacts [20]. Here, the heart is treated as a single current dipole source in the thorax modelled to have a uniform electrical conductivity with air added as electrical insulation as the boundary [21]. In our computational model using COMSOL software, the current-source dipole heart model is surrounded by a homogeneous volume conductor (average tissue conductivity = 0.33 S/m) with the shape of a three-dimensional human torso, consisting of 2 mm<sup>3</sup> elements (Fig. 1D). The magnitude of the electric current dipole moment is assumed to be 1 (mA meter) [22]. This model was solved linearly through finite element methods (FEM). To simulate the maximum possible artifact value, the hypothetical locations of the dipole points are examined in different scenarios around the heart locus. The net voltage induced across the lead was then calculated by integrating the electric field between device location and leads placed in the center of the cranium.

## 3. Results

### 3.1. Empirical artifact incidence

Visual inspection of LFP recorded in subclavicular implants (N = 54, all Medtronic Percept, see Fig. 1A for exemplar traces) revealed higher proportion of overall ECG contaminated signals (Fig. 1B) in left (58/89 channels, 65.2%, N = 23 devices) vs. right implants (41/118 channels, 34.8%, N = 31 devices,  $p = 0.006$ ). Importantly, severe ECG contamination, most likely rendering the signals unusable for therapeutic algorithms, were three times more likely to occur in left (43/89, 48.3%, N = 23) vs. right implant locations (18/118, 15.3%, N = 31,  $p = 0.001$ ). Given that each patient has 2 potential recording channels per lead, the availability of at least one useable signal stream per lead and hemisphere is particularly relevant for recruitment and planning of clinical aDBS trials. For bilateral use, at least one unaffected channel per hemisphere and lead is required (Fig. 1C). This was the case in only 45.5% (10/22) of patients with left, compared to 89.3% (25/28,  $p = 0.002$ ) patients with right implants and two connected leads (unilateral implants excluded). If unilateral recordings were to prove sufficient for bilateral control of the stimulator in aDBS this would have been possible in 63.6% of left implants (14/22) and 96.4% of right implants (27/28,  $p = 0.008$ ). In the sub-cohort of 13 patients (9/4 left/right implants) 17/52 channels were contaminated with ECG when recordings were performed with the IPG coupled (stimulation ready) as the stimulation anode, but only 1 channel was contaminated without coupling (1/52;  $p = 0.016$ ), which confirms the role of the IPG case as a parasitic reference.

ECG was absent in neural data from cranial implants (32 patients, 128 channels, all RNS Neuropace), yielding a significant difference to both left and right subclavicular implants (all  $p < 0.01$ ).

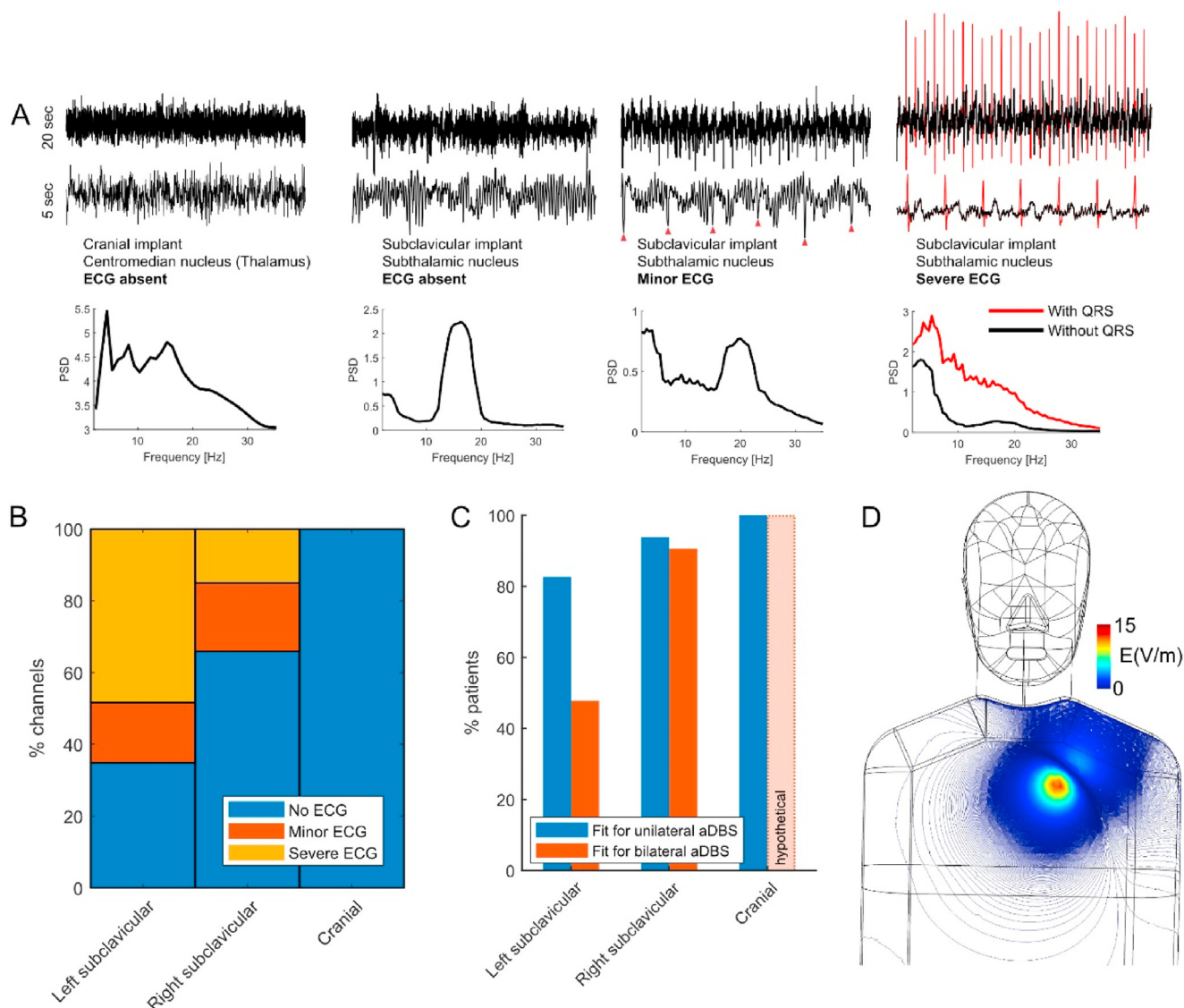


**Fig. 1.** ECG artifacts contaminate neural signals in subclavicular implants. Exemplar thalamic and subthalamic LFP and resulting power spectral densities (A) recorded from patients with Epilepsy (cranial implant targeting the Centromedian nucleus of thalamus) and Parkinson's disease (subclavicular implant targeting subthalamic nucleus) demonstrate the artifact categories (absent, minor, severe from left to right). For offline processing, the QRS complex can be identified (e.g. red arrow in minor contamination) and removed (red line in severe contamination category, see <https://github.com/neuromodulation/perceive>). In the severe contamination example replacing 4.37 s affected by QRS (red high amplitude discharges) with mirrored padding could restore an underlying beta oscillatory peak (black PSD), demonstrating the severity of beta frequency contamination from the QRS complex alone (red PSD). ECG contaminated channels were present in left and right subclavicular implants (B), rendering a significant portion of DBS leads unusable for aDBS trials (C). Modeling the electric field (D) throughout the cardiac cycle suggests a higher susceptibility for ECG artifacts in the left, when compared to right chest. Note, that the IPG itself is unlikely to lead to large changes in this distribution and was not modelled for the present figure. (For interpretation of the references to colour in this figure legend, the reader is referred to the Web version of this article.)

### 3.2. Electric field models estimate peak ECG contamination and relative susceptibility

The induced voltage at the measurement leads is estimated by integrating the electric fields, approximated using FEM to be 15.2 V/m for subclavicular (Fig. 1D) and 94  $\mu\text{V}/\text{m}$  for cranial implant regions (with respective current densities of 5.02  $\text{A}/\text{m}^2$  and 42.7  $\mu\text{A}/\text{m}^2$ ). The resulting cardiac artifacts are estimated to be approximately 1 mV for a chest mounted device, with a relative artifact 4.1 and 6.5 times greater for the left compared to right side due to differences in the net integrated electrical field. The cranial mounted system results in an estimated artifact signal of approximately 100 nV.

The cardiac artifact is presented as a common-mode signal to the pre-amplifier. The worst-case susceptibility arises during passive recharge since this state creates a direct connection to the implantable case and presents the ECG artifact to the input chain. The net artifact that couples into the signal chain depends on the common mode rejection ratio (CMRR) of the sensing interface, which can range from  $-80$  to  $-40$  dB depending on the matching characteristics of the electrode-lead-extension-amplifier pathway [19]. Based on the modest CMRR, artifact amplitude is expected to exceed the LFP ( $\sim 1\text{--}20$   $\mu\text{V}_{\text{rms}}$ ) in chest-mounted devices for a sizeable proportion of systems; the exact proportion depending on the distribution of CMRR. In cranial mount devices, the artifact is

**Table 1**  
Subclavicular implant details.

| Left subclavicular implants |     |      |        |         | Right subclavicular implants |     |     |        |         |
|-----------------------------|-----|------|--------|---------|------------------------------|-----|-----|--------|---------|
| N                           | DIS | TGT  | BAD CH | BAD HEM | N                            | DIS | TGT | BAD CH | BAD HEM |
| 1 <sup>-</sup>              | DYT | GPI  | 3      | 2       | 1                            | PD  | STN | 2      | 0       |
| 2                           | DYT | GPI  | 2      | 1       | 2                            | PD  | STN | 0      | 0       |
| 3                           | PD  | STN  | 1      | 0       | 3                            | PD  | STN | 0      | 0       |
| 4                           | PD  | STN  | 0      | 0       | 4                            | PD  | STN | 0      | 0       |
| 5                           | PD  | STN  | 1      | 0       | 5                            | PD  | GPI | 0      | 0       |
| 6                           | PD  | STN  | 1      | 0       | 6                            | PD  | GPI | 0      | 0       |
| 7                           | PD  | STN  | 4      | 2       | 7                            | PD  | GPI | 0      | 0       |
| 8                           | PD  | STN  | 3      | 1       | 8                            | PD  | GPI | 1      | 0       |
| 9                           | PD  | STN  | 0      | 0       | 9                            | PD  | STN | 0      | 0       |
| 10                          | PD  | STN  | 4      | 2       | 10                           | PD  | STN | 1      | 0       |
| 11                          | PD  | GPI  | 3      | 1       | 11                           | DYT | GPI | 0      | 0       |
| 12                          | PD  | STN  | 0      | 0       | 12                           | PD  | STN | 0      | 0       |
| 13                          | PD  | STN  | 0      | 0       | 13                           | PD  | STN | 0      | 0       |
| 14 <sup>#</sup>             | DYT | GPI  | 4      | 2       | 14                           | PD  | STN | 0      | 0       |
| 15                          | PD  | STN  | 4      | 2       | 15                           | PD  | GPI | 0      | 0       |
| 16                          | PD  | STN  | 0      | 0       | 16                           | OCD | AIC | 1      | 0       |
| 17 <sup>*</sup>             | PD  | GPI  | 0      | 0       | 17                           | PD  | GPI | 4      | 2       |
| 18 <sup>§</sup>             | TIN | CAUD | 2      | 1       | 18                           | PD  | GPI | 0      | 0       |
| 19                          | PD  | STN  | 2      | 0       | 19                           | ET  | VIM | 0      | 0       |
| 20                          | ET  | VIM  | 3      | 1       | 20                           | PD  | GPI | 0      | 0       |
| 21                          | PD  | STN  | 0      | 0       | 21 <sup>*#</sup>             | DYT | GPI | 0      | 0       |
| 22                          | PD  | STN  | 3      | 1       | 22 <sup>*</sup>              | DYT | GPI | 0      | 0       |
| 23                          | PD  | STN  | 3      | 1       | 23 <sup>*</sup>              | PD  | GPI | 1      | 0       |
|                             |     |      |        |         | 24                           | PD  | GPI | 1      | 0       |
|                             |     |      |        |         | 25                           | PD  | STN | 2      | 1       |
|                             |     |      |        |         | 26                           | DYT | GPI | 0      | 0       |
|                             |     |      |        |         | 27                           | DYT | GPI | 4      | 2       |
|                             |     |      |        |         | 28                           | PD  | STN | 1      | 0       |
|                             |     |      |        |         | 29                           | DYT | GPI | 0      | 0       |
|                             |     |      |        |         | 30                           | PD  | STN | 0      | 0       |
|                             |     |      |        |         | 31                           | ET  | VIM | 0      | 0       |

Abbreviations: AIC = anterior limb of internal capsule; BAD CH = Number of channels with severe ECG contamination; BAD HEM = Number of hemispheres with all channels with severe ECG contamination; CAUD = Caudate nucleus; DIS = Disease; DYT = Dystonia, ET = Essential Tremor; GPI = internal pallidum; OCD = obsessive compulsive disorder; PD = Parkinson's disease; STN = subthalamic nucleus; TGT = Target; TIN = Tinnitus; VIM = ventral intermediate nucleus of thalamus; <sup>§</sup>one channel excluded; <sup>\*</sup> unilateral implants; <sup>#</sup> depict two separate percept implants in a single patient; <sup>-</sup> abdominal implants.

predicted to be below the amplifier noise floor (~100nV/rt-Hz) and undetectable in all current commercial devices.

**4. Discussion**

The present study demonstrates that ECG contamination of neural signals recorded with novel implantable devices is related to proximity of the device to the electric field of the heart. We derive three major consequences from this. First, for subclavicular systems, the device is highly susceptible to its location relative to the cardiac dipole. In practice, patients with left implants are more likely to exhibit ECG in neural recordings than patients with right implants. From our empirical data, only 45% of patients with left hemibody implants were fit for bilateral adaptive stimulation, compared to 89% in patients with right implants. The second implication is that even right subclavicular implants can suffer from ECG contamination. The third implication is that recordings in monopolar stimulation mode (or during calibration test) have significantly higher probability of ECG contamination than recordings in pure sensing mode (not stimulation-ready), due to coupling of the DBS anode to the IPG. Therefore, direct comparisons of stimulation ON vs. OFF can be biased through ECG susceptibility, which can be obviated by defining the same stimulation montage but leaving stimulation amplitude at 0 mA for stimulation OFF condition recordings. This problem is exacerbated by the use of passive recharge for stimulation, which extends the time that the IPG case is coupled as the anode; passive recharge is desired to minimize power and reverting to active recharge would undermine the potential energy savings of adaptive stimulation.

Beyond aDBS for Parkinson's disease, electrophysiological biomarkers that are also susceptible to these artifacts have been described in dystonia [23,24], essential tremor [25], Tourette's syndrome [26,27] and other neuropsychiatric disorders [28]. Further technical improvements for artifact suppression are required to offer new therapeutic advances to all DBS patients.

*4.1. Origin of susceptibility to artifacts in brain sensing interfaces*

Local field potentials are measured as a differential signal from the leads implanted in the brain. The LFP signal can range from 1 to 20 μVrms [19], and the majority of LFP oscillations are in low frequency bands, ranging from 1 Hz to 100 Hz, where artifacts are also present [16]. When a DBS device is implanted, the device case can act, sometimes inadvertently, as the system's reference. In theory, the ECG artifact would be rejected by the sensing input chain as a common mode signal. In an implantable system, however, the common mode rejection ratio can be undermined by sources of mismatch. Such mismatch can occur due to variation in 1) the tissue-electrode interface, 2) impedance along the lead and extension interfaces 3) interface filter components, and 4) the sensing amplifier. The mismatching allows for a finite amount of common-mode signal to enter the differential signal chain.

*4.2. Mitigation of ECG contamination in neural recordings from implantable devices*

Our study suggests that strategic placement distant to the cardiac electric dipole can partially mitigate ECG contamination by

limiting its amplitude. We should note that there are alternative approaches to address artifact susceptibility. Importantly, our reasoning suggests that bipolar stimulation montages could mitigate ECG, as has been reported in a recent study investigating a different device [28]. However, bipolar stimulation may lead to other artifact problems by creating a differential stimulation artifact as seen by the sensing chain. In the future, alternative methods for artifact mitigation include 1) improving the matching of the signal chain by improving the electrical properties of leads and extensions, 2) lowering the tissue-electrode interface impedance with new coatings 3) exploring alternative signals at frequencies outside of the artifact susceptibility such as evoked potentials [29], or 4) using sources such as electrocorticography with larger signal amplitudes [12,30–34]. One or more of these might be adopted in future systems. Finally, given the characteristics of the high amplitude QRS component, post-hoc processing can restore a significant portion (~80%) underlying neural activity in many contaminated signals; this approach could prove possible in real-time if achievable with acceptable power consumption [35].

#### 4.3. Limitations

The evaluation of ECG artifact was visual, which has the potential for subjective bias. In the future we hope to validate our findings with objective measurements of ECG contamination relative to adaptive algorithm requirements. Importantly, even though we demonstrate data from a representative sample size, we only included data recorded from a single device for subclavicular (Medtronic Percept) and cranial (RNS Neuropace) implants. However, a previous generation of subclavicular devices (Medtronic PC + S) had corrupted recording streams often excluded them from otherwise valuable studies [17,18]. For cranial implants, higher amplitude signals from cortical recording locations are additionally beneficial and may represent a bias in the ECG contamination statistic. It is worth noting that although our focus was on ECG artifacts, susceptibility to motion artifacts raises similar issues that could limit algorithms (see Supplementary Fig. 1 for exemplar data traces), but the root cause of these artifacts remains under investigation and could include new processes such as triboelectric phenomena.

In conclusion, sensing enabled IPGs for neurostimulation can suffer from ECG contamination that is larger and more frequent in left subclavicular implant locations, when compared to right-sided or cranial implants. Mitigation strategies include adjustment of implant location, alternative higher amplitude signal sources and post-hoc processing [34]. Given the absence of ECG in cranial implants, our data suggest that future bidirectional brain computer interfaces should explore the utility of cranial mounts to avoid ECG contamination altogether.

#### Authorship CRediT statement

WJN and TD conceptualized the study, performed statistical analysis, and drafted the manuscript. MMS, MB, PB and TD conceptualized and performed the modeling analysis. LKF, AS, JKK, MFC, TS, RJ, GT, CP, IUI, DDC, SL, PS, VK, GH, TH, RMR and AAK acquired, curated and analysed electrophysiological data. AAK and TD provided funding and project administration for the study. WJN and TD wrote the first draft of the manuscript. All authors revised and approved the final version of the manuscript.

#### Acknowledgements

The authors would like to thank Dr. R. Zutt (Dept. of Neurology Hagaziekenhuis), Dr. N.A. van der Gaag, and Dr. C.F Hoffmann (Dept

of Neurosurgery, Hagaziekenhuis) for the clinical care of the patients and help with data acquisition. This study was funded by the Deutsche Forschungsgemeinschaft (DFG, German Research Foundation) – Project-ID 424778381 – TRR 295 to WJN, IUI and AAK, the Bundesministerium für Bildung und Forschung (BMBF, FKZ01GQ1802) to WJN, the Medical Research Council, United Kingdom (MC\_UU\_12024/1) to PB, the Czech Ministry of Education under grant AZV: NV19-04-00233 and by Charles University under research project Progres Q27 to RJ.

#### Appendix A. Supplementary data

Supplementary data to this article can be found online at <https://doi.org/10.1016/j.brs.2021.08.016>.

#### References

- [1] Cagnan H, Denison T, McIntyre C, Brown P. Emerging technologies for improved deep brain stimulation. *Nat Biotechnol* 2019;37:1024–33. <https://doi.org/10.1038/s41587-019-0244-6>.
- [2] Krauss JK, Lipsman N, Aziz T, Boutet A, Brown P, Chang JW, et al. Technology of deep brain stimulation: current status and future directions. *Nat Rev Neurol* 2020. <https://doi.org/10.1038/s41582-020-00426-z>.
- [3] Little S, Pogosyan A, Neal S, Zavala B, Zrinzo L, Hariz M, et al. Adaptive deep brain stimulation in advanced Parkinson disease. *Ann Neurol* 2013. <https://doi.org/10.1002/ana.23951>.
- [4] Arlotti M, Marceglia S, Foffani G, Volkman J, Lozano AM, Moro E, et al. Eight-hours adaptive deep brain stimulation in patients with Parkinson disease. *Neurology* 2018. <https://doi.org/10.1212/WNL.0000000000005121>.
- [5] Meidahl AC, Tinkhauser G, Herz DM, Cagnan H, Debarros J, Brown P. Adaptive deep brain stimulation for movement disorders: the long road to clinical therapy. *Mov Disord* 2017;32:810–9. <https://doi.org/10.1002/mds.27022>.
- [6] Rosin B, Slovik M, Mitelman R, Rivlin-Etzion M, Haber SN, Israel Z, et al. Closed-loop deep brain stimulation is superior in ameliorating parkinsonism. *Neuron* 2011;72:370–84. <https://doi.org/10.1016/j.neuron.2011.08.023>.
- [7] Neumann W-J, Degen K, Schneider G-H, Brücke C, Huebel J, Brown P, et al. Subthalamic synchronized oscillatory activity correlates with motor impairment in patients with Parkinson's disease. *Mov Disord* 2016;31:1748–51. <https://doi.org/10.1002/mds.26759>.
- [8] Kuhn AA, Kupsch A, Schneider GH, Brown P. Reduction in subthalamic 8–35 Hz oscillatory activity correlates with clinical improvement in Parkinson's disease. *Eur J Neurosci* 2006;23. France.
- [9] Kehnemouyi YM, Wilkins KB, Anidi CM, Anderson RW, Afzal MF, Bronte-Stewart HM. Modulation of beta bursts in subthalamic sensorimotor circuits predicts improvement in bradykinesia. *Brain* 2020. <https://doi.org/10.1093/brain/awaa394>.
- [10] Eusebio A, Thevathasan W, Doyle Gaynor L, Pogosyan A, Bye E, Foltynie T, et al. Deep brain stimulation can suppress pathological synchronisation in parkinsonian patients. *J Neurol Neurosurg Psychiatry* 2011;82:569–73.
- [11] Kühn AA, Kempf F, Brücke C, Gaynor Doyle L, Martinez-Torres I, Pogosyan A, et al. High-frequency stimulation of the subthalamic nucleus suppresses oscillatory beta activity in patients with Parkinson's disease in parallel with improvement in motor performance. *J Neurosci* 2008;28:6165–73.
- [12] Neumann W-J, Turner RS, Blankertz B, Mitchell T, Kühn AA, Richardson RM. Toward electrophysiology-based intelligent adaptive deep brain stimulation for movement disorders. *Neurotherapeutics* 2019;16. <https://doi.org/10.1007/s13311-018-00705-0>.
- [13] Kokkinos V, Sisterson ND, Wozny TA, Richardson RM. Association of closed-loop brain stimulation neurophysiological features with seizure control among patients with focal epilepsy. *JAMA Neurol* 2019;76:800–8. <https://doi.org/10.1001/jamaneurol.2019.0658>.
- [14] Neumann WJ, Turner RS, Blankertz B, Mitchell T, Kühn AA, Richardson RM. Toward electrophysiology-based intelligent adaptive deep brain stimulation for movement disorders. *Neurotherapeutics* 2019. <https://doi.org/10.1007/s13311-018-00705-0>.
- [15] Kühn AA, Volkman J. Innovations in deep brain stimulation methodology. *Mov Disord* 2017 Jan;32(1):11–9. <https://doi.org/10.1002/mds.26703>. Epub 2016 Jul 12.
- [16] Thakor NV. From holter monitors to automatic defibrillators: developments in ambulatory arrhythmia monitoring. *IEEE Trans Biomed Eng* 1984. <https://doi.org/10.1109/TBME.1984.325237>. BME-31:770–8.
- [17] Anidi C, O'Day JJ, Anderson RW, Afzal MF, Sytkin-Nikolau J, Velisar A, et al. Neuromodulation targets pathological not physiological beta bursts during gait in Parkinson's disease. *Neurobiol Dis* 2018;120:107–17. <https://doi.org/10.1016/j.nbd.2018.09.004>.
- [18] Neumann WJ, Staub-Bartelt F, Horn A, Schanda J, Schneider GH, Brown P, et al. Long term correlation of subthalamic beta band activity with motor impairment in patients with Parkinson's disease. *Clin Neurophysiol* 2017. <https://doi.org/10.1016/j.clinph.2017.08.028>.

- [19] Stanslaski S, Afshar P, Cong P, Giftakis J, Stypulkowski P, Carlson D, et al. Design and validation of a fully implantable, chronic, closed-loop neuromodulation device with concurrent sensing and stimulation. *IEEE Trans Neural Syst Rehabil Eng* 2012;20:410–21. <https://doi.org/10.1109/TNSRE.2012.2183617>.
- [20] Sorkhabi MM, Benjaber M, Brown P, Denison T. Physiological artifacts and the implications for brain-machine-interface design. *IEEE Int. Conf. Syst. Man, Cybern., IEEE*; 2020. <https://doi.org/10.1109/SMC42975.2020.9283328>. 2020, p. 1498–1498.
- [21] Feher JJ. 5.6 - the electrocardiogram. *Quant. Hum. Physiol. An introd.. Academic Press*; 2012. p. 467–76.
- [22] Nomura M, Nakaya Y, Miyoshi Y, Wakatsuki T, Saito K, Bando S, et al. Single moving dipole obtained from magnetic field of the heart in patients with left ventricular hypertrophy. *Clin Cardiol* 1992;15:752–8. <https://doi.org/10.1002/CLC.4960151013>.
- [23] Neumann W-J, Horn A, Ewert S, Huebl J, Brücke C, Slentz C, et al. A localized pallidal physiomaerker in cervical dystonia. *Ann Neurol* 2017;82:912–24. <https://doi.org/10.1002/ana.25095>.
- [24] Neumann W-J, Huebl J, Brücke C, Ruiz MH, Kupsch A, Schneider G-H, et al. Enhanced low-frequency oscillatory activity of the subthalamic nucleus in a patient with dystonia. *Mov Disord* 2012;27. <https://doi.org/10.1002/mds.25078>.
- [25] Tan H, Debarros J, He S, Pogosyan A, Aziz TZ, Huang Y, et al. Decoding voluntary movements and postural tremor based on thalamic LFPs as a basis for closed-loop stimulation for essential tremor. *Brain Stimul* 2019;12: 858–67. <https://doi.org/10.1016/j.brs.2019.02.011>.
- [26] Neumann W-J, Huebl J, Brücke C, Lofredi R, Horn A, Saryyeva A, et al. Pallidal and thalamic neural oscillatory patterns in Tourette syndrome. *Ann Neurol* 2018. <https://doi.org/10.1002/ana.25311>.
- [27] Molina R, Okun MS, Shute JB, Opri E, Rossi PJ, Martinez-Ramirez D, et al. Report of a patient undergoing chronic responsive deep brain stimulation for Tourette syndrome: proof of concept. *J Neurosurg* 2017;1–7. <https://doi.org/10.3171/2017.6.jns.17626>.
- [28] Neumann W-J, Huebl J, Brücke C, Gabriëls L, Bajbouj M, Merkl A, et al. Different patterns of local field potentials from limbic DBS targets in patients with major depressive and obsessive compulsive disorder. *Mol Psychiatr* 2014;19. <https://doi.org/10.1038/mp.2014.2>.
- [29] Sinclair NC, McDermott HJ, Bulluss KJ, Fallon JB, Perera T, Xu SS, et al. Subthalamic nucleus deep brain stimulation evokes resonant neural activity. *Ann Neurol* 2018;83:1027–31. <https://doi.org/10.1002/ana.25234>.
- [30] Swann NC, De Hemptinne C, Thompson MC, Miocinovic S, Miller AM, Gilron R, et al. Adaptive deep brain stimulation for Parkinson's disease using motor cortex sensing. *J Neural Eng* 2018. <https://doi.org/10.1088/1741-2552/aabc9b>.
- [31] Opri E, Cernera S, Molina R, Eisinger RS, Cagle JN, Almeida L, et al. Chronic embedded cortico-thalamic closed-loop deep brain stimulation for the treatment of essential tremor. *Sci Transl Med* 2020;12:eaay7680. <https://doi.org/10.1126/scitranslmed.aay7680>.
- [32] Gilron R, Little S, Perrone R, Wilt R, Hemptinne C De, Yaroshinsky MS, et al. Long-term wireless streaming of neural recordings for circuit discovery and adaptive stimulation in individuals with Parkinson's disease. *Nat Biotechnol* 2021;1–22. <https://doi.org/10.1038/s41587-021-00897-5>.
- [33] Houston B, Thompson M, Ko A, Chizeck H. A machine-learning approach to volitional control of a closed-loop deep brain stimulation system. *J Neural Eng* 2019;16. <https://doi.org/10.1088/1741-2552/aae67f>.
- [34] Johnson V, Wilt R, Gilron R, Anso J, Perrone R, Beudel M, et al. Embedded adaptive deep brain stimulation for cervical dystonia controlled by motor cortex theta oscillations. *Exp Neurol* 2021;113825. <https://doi.org/10.1016/J.EXPNEUROL.2021.113825>.
- [35] Chen Y, Ma B, Hao H, Li L. Removal of electrocardiogram artifacts from local field potentials recorded by sensing-enabled neurostimulator. *Front Neurosci* 2021;15:226. <https://doi.org/10.3389/FNINS.2021.637274>.